Journal of Environmental Chemical Engineering 2 (2014) 1831–1840

Contents lists available at ScienceDirect

Journal of Environmental Chemical Engineering

journal homepage: www.elsevier.com/locate/jece

Virus removal by iron oxide ceramic membranes

Maria M. Fidalgo de Cortalezzi [a,d,*], Maria V. Gallardo [a], Fernando Yrazu [a], Guillermina J. Gentile [a], Oscar Opezzo [a,b], Ramon Pizarro [a,b], Hugo R. Poma [c,d], Verónica B. Rajal [c,d]

[a] Department of Chemical Engineering, Instituto Tecnológico de Buenos Aires, Avenue Madero 399, 1106 Buenos Aires, Argentina
[b] Comisión Nacional de Energía Atómica, Unidad de Actividad Radiobiología, Avenue General Paz 1499, General San Martín, 1650 Buenos Aires, Argentina
[c] INIQUI, Universidad Nacional de Salta, Avenue Bolivia 5150, 4400 Salta, Argentina
[d] CONICET, Argentina

ARTICLE INFO

Article history:
Received 29 May 2014
Accepted 2 August 2014
Available online 7 August 2014

Keywords:
Ceramic membranes
Iron oxides
Nanoparticles
Viral contamination
Water treatment

ABSTRACT

Nanoporous iron oxide ceramics were studied for the removal of virus contamination from water. Supported and unsupported iron oxide nanostructured hematite was fabricated by a green chemistry route from ferroxane nanoparticles. The material had a surface area of approximately 30 m^2/g and a mean pore size of 65 nm. Bacteriophage P22 was chosen as a model for human virus. The kinetics and equilibrium of the attachment process was investigated. P22 adsorption isotherms on iron oxide were described by the Freundlich equation. Batch experiments resulted in 1.5 LRVs. Removal proceeded rapidly for the first 7 h; next, a diffusion-limited stage occurred. Dynamic attachment experiments demanded extensive recirculation to achieve significant reduction levels. Up to 3 LRV were observed. The enhanced performance can be explained by the higher iron oxide area available and the facilitated access to inner porosity sites that were previously unavailable due to slow diffusion. The role of electrostatic interactions in the attachment mechanisms was confirmed by the dependence of the isotherm on the ionic strength of the suspension medium. P22 bacteriophage is expected to attach to the iron oxide by electrostatic forces up to a pH of 6.5. DLVO theory predicts moderately well the interaction energies between P22 particles themselves and between the phage and the ceramic. However, a slight underestimation of the P22–P22 repulsive forces was evident by comparison to the experimental data.

Introduction

The availability of a safe water supply is an increasingly important priority for the welfare and development of human populations, challenged by the combined growth of demography, development, and waste. Parallel to this, researchers and authorities have been paying more attention in the last decades to the link between disease outbreaks and the presence of viral pathogens in drinking water sources [1]. The removal or inactivation of virus in water treatment is a challenging task: the technical difficulty resides in the fact that viruses and bacterial spores are much harder to eliminate -by common techniques such as microfiltration or chlorination for example- than bacterial pathogens due to their smaller size and simpler physiology. Although bacteria and larger microorganisms can be removed by ultrafiltration or microfiltration, the removal of smaller viral particles is mainly controlled by electrostatic interactions and attachment [2,3]. Nanofiltration membranes meet the requirements for nanosize particle removal, but its use represents a significant increase in cost due to higher pressure requirements and lower produced water yields [4]. Consequently, there is a need to develop cost-efficient methods to achieve these goals, not only for large urban agglomerations but also for smaller rural populations and mobile applications.

Adsorption processes can effectively remove small contaminants as well as ionic constituents from water, avoiding energy consumption associated with pumping and disposal issues of concentrated streams generated [5,6]. Furthermore, bulk porous adsorbents, as opposed to suspended colloidal particles and co-precipitation schemes, offer the additional advantage of not requiring an extra separation stage added to the treatment process, and thus, rendering the system safer to handle, easier to use and applicable to mobile devices. In order for an adsorbent to be an

* Corresponding author. Current address: E2509 Laferre Hall, Department of Civil and Environmental Engineering, University of Missouri-Columbia, Columbia, MO 65211-2200, USA. Tel.: +1 573 884 6777.
E-mail addresses: fidalgom@missouri.edu, maria.fidalgo1@gmail.com (M.M. Fidalgo de Cortalezzi).

http://dx.doi.org/10.1016/j.jece.2014.08.006
2213-3437/

Nomenclature

a	radius of virus like particle (m)
A_{132}	combined Hamaker constant for bacteriophage P22 and hematite in water as medium (J)
A_{131}	Hamaker constant for bacteriophage P22 in water as medium (J)
A_{11}	Hamaker constant of virus like particle (J)
A_{22}	Hamaker constant of hematite (J)
A_{33}	Hamaker constant of water (J)
C	ion concentration (mol dm^{-3})
DLVO	Derjaguin
Landau	Verwey and Overbeek
e	electron charge
h	separation between surfaces (m)
k	Boltzmann constant
n_∞	bulk number of ions (ions m^{-3})
T	temperature (K)
U	electrophoretic mobility (m^2 V^{-1} s^{-1})
V_{EDL}	electrical double layer interaction potential energy (J)
V_{TOTAL}	total colloidal interaction potential energy (J)
V_{vdW}	unretarded van der Waals interaction potential energy (J)
z	valence of symmetrical (z–z) electrolyte
z_i	valence of ion i including sign of charge
γ	reduced surface potential
ε	dielectric constant (F m^{-1})
ε	permittivity
ζ	zeta potential (V)
κ	Debye–Huckel reciprocal length (m^{-1})
μ	viscosity (Pa s)
φ	electrical surface potential (V)

efficient and economically sound option while still maintaining the above mentioned characteristics, it must be readily available on site, have a relatively high specific surface area, low cost, and no toxicity associated with its fabrication, use, or final disposal of the material itself or its degradation products.

Previous work successfully led to the developing of iron oxide nanostructured ceramic membranes [7,8], which have proven to be an efficient treatment for the removal of natural arsenic contamination [9] and promising for other ionic contaminants as well. These membranes are specially suited for their use as filters of both inorganic/organic and biological contaminants in rural settings where access to electricity or specialized supplies is compromised. There is evidence [10–12] that iron and iron oxides can effectively retain and/or inactivate viral particles. Furthermore, iron oxides or minerals having a substantial proportion of iron oxides have shown very high affinity for virus that seems to be independent of their type or structure [10,13], and therefore can become a general method for the removal of virus from natural waters, where microorganisms exhibit seasonal and special variability [14,15]. Metal oxide coatings on sand [16–19], glass fiber [20,21], ceramic filters [22,23], and diatomaceous earth [24] have been used in the removal and inactivation of virus from water.

Bacteriophages are recognized as model organisms for human virus [25,26]. P22 [27] and MS2 [13] phages have been used in attachment experiments as well as other phages [28]. P22 phage has an icosahedral capsid and an approximate diameter of 70 nm, which is within the same order of magnitude as picornaviruses, the wide family to which human enteroviruses belong (approximately 30 nm) [29–31].

The nanostructured iron oxide ceramic filter investigated in this work presents numerous advantages over previously studied systems: ease of operation, low fabrication cost, more compact due to the higher specific active area available, and no sludge generation. The attachment kinetics and equilibrium isotherm of bacteriophage P22 was investigated. The virus was characterized with respect to size and surface charge, as they are expected to play a key role in the removal process. A flow through ceramic filter was fabricated and tested for the continuous treatment of contaminated water. The mechanism and limitations of the processes were analyzed and discussed in light of the DLVO theory of colloidal interaction, as well as the aggregation conditions of the phage in natural waters.

Theory

DLVO theory, developed independently by Derjaguin and Landau (1941) and by Verwey and Overbeek (1948), explains colloid stability as well as attachment between colloids and surfaces, based on the van der Waals attraction and the electrical double layer repulsion.

When there is a particle in aqueous suspension that presents surface charge, as for example due to ionization of surface chemical groups, a layer of counterions will develop to balance the charge in the solution adjacent to the surface and an electrical double layer surrounding the particle will appear. As two particles approach, the double layers overlap, giving origin to interaction forces.

The electrical double layer interaction potential energy between two spheres can be calculated by the following expression [32]:

$$V_{EDL} = \frac{128\pi a_1 a_2 n_\infty kT}{(a_1 + a_2)\kappa^2}\gamma_1\gamma_2 \exp(-\kappa h) \quad (1)$$

$$\gamma = \tanh\frac{ze\varphi}{4kT} \quad (2)$$

where V_{EDL}: electrical double layer interaction potential energy (J), a: radius of virus like particle (m), n_∞: bulk number of ions (ions m^{-3}), k: Boltzmann constant (1.38×10^{-23} J/K), T: temperature (K), κ: Debye–Huckel reciprocal length (m^{-1}), γ: reduced surface potential, z: valence of symmetrical (z–z) electrolyte, e: electron charge (-1.602×10^{-19} C), φ: electrical surface potential (V), h: separation between surfaces (m).

This equation is valid when $h \ll a$ and $\kappa h \gg 5$; in a symmetric electrolyte solution.

In aqueous solutions at 25 °C, κ can be calculated as [33]

$$\kappa = 2.32 \times 10^9 \sqrt{\sum C_i z_i^2} \quad (3)$$

where C_i: ion concentration (mol dm^{-3}).

If there is a large difference between particle sizes, the bigger one is perceived as an infinite plate, and Eq. (1) reduces to:

$$V_{EDL} = \frac{128\pi a n_\infty kT}{\kappa^2}\gamma_1\gamma_2 \exp(-\kappa h) \quad (4)$$

The electrical surface potential (φ) is commonly approximated by the zeta potential (potential at the shear plane) due to the impossibility to experimentally determine the first.

Attractive van der Waals interactions are the result of short-term magnetic forces that form between identical or different particles that may have the same, different or no net charge, due to transition dipoles, and depend on the geometry, properties of the particles and the medium in which they interact.

For two identical interacting spheres, the potential can be calculated according to [34]:

$$V_{vdW} = -\frac{A_{131}}{6}\left(\frac{2a_1a_2}{h^2+2a_1h+2a_2h}+\frac{2a_1a_2}{h^2+2a_1h+2a_2h+4a_1a_2} + \ln\frac{h^2+2a_1h+2a_2h}{h^2+2a_1h+2a_2h+4a_1a_2}\right) \quad (5)$$

where V_{vdW}: unretarded van der Waals interaction potential energy (J), A_{131}: Hamaker constant for two spheres of material 1 suspended in a medium 3 (J).

For a sphere-plate geometry [34]:

$$V_{vdW} = -\frac{A_{132}}{6}\left(\frac{a}{h}+\frac{a}{h+2a}+\ln\frac{a}{h+2a}\right) \quad (6)$$

where A_{132}: combined Hamaker constant for the sphere 1 and the plate 2 in a specific medium 3 (J).

DLVO theory considered the total potential energy of interaction as the sum of both electrical double layer and van der Waals potential:

$$V_{TOTAL} = V_{EDL} + V_{vdW} \quad (7)$$

Additional non-DLVO interacting forces (e.g., Born repulsion, hydration forces, hydrophobic and/or steric forces, polymer bridging) may also exist but they can be assumed to be negligible in many cases in comparison with electric double layer and van der Waals potential energies.

Materials and methods

Materials

All chemicals were of reagent grade, except $FeCl_2$ used in the synthesis of the iron nanoparticles that was technical grade. Solutions were prepared in all cases using type I (18 MΩ) water.

P22 phage stock suspensions had a concentration of approximately 2×10^{10} pfu/mL [35]. Viral solutions and subsequent dilutions were made by dissolving NaCl (Anedra, Argentina) in DI water to obtain a 15 mM concentration. The culture media used in these experiments were LB broth Lenox and LB Agar Lenox with two different concentrations of agar–agar as presented in Table 1. In order to provide the inoculum for each plaque, *Salmonella* typhimurium strain DA1468, was spiked in 10 mL of LB broth Lenox, and then incubated for 24 h at 37 °C.

Glassware, tips, eppendorf tubes, adsorbent and inert solutions were sterilized by autoclaving at 121 °C for 15 min. Micropipettes were thoroughly rubbed with ethanol 70% prior to usage.

Purification of bacteriophage P22

After replication, the virus suspension was centrifuged at 15,000 rpm for 60 min. Then, the supernatant was filtered through a 0.22 μm PVDF membrane (Millipore GVW P02500). This suspension was dialyzed through a 100 kDa MWCO membrane (SpectraPor Biotech CE, Spectrum Laboratories, USA) twice: first, against Milli-Q water, and secondly, against a 15 mM NaCl solution for 20 h each. The final suspension was filtered again and kept at 4 °C.

Table 1
Culture media and solutions used in virus experiments.

	L brotth	Soft L agar	L agar	Brand	Lot
Tryptone (g/L)	10	10	10	Britania	687
Yeast extract (g/L)	5	5	5	Britania	550.3
Agar–Agar (g/L)	0	7.5	15	Britania	238
Sodium chloride (g/L)	5	5	5	Anedra	17872.1

Synthesis of ferroxane nanoparticles

Iron oxide nanoparticles were synthesized in the laboratory following previously published procedure [9]. Briefly, lepidocrocite was obtained by oxidation of $FeCl_2$ (PPE, Argentina) under controlled pH. NaOH (Anedra, Argentina) was used for pH adjustments. Secondly, the prepared lepidocrocite was reacted with anhydrous acetic acid (Anedra, Argentina) to yield ferroxane nanoparticles by the attack of the acid on the hydrogen bonds of the mineral structure. These nanoparticles are precursors to ceramic membranes; they can be either deposited onto support matrices or used as a self-standing material. Finally, the ferroxane particles were sintered at 450 °C and converted to iron oxide ceramic (hematite).

Characterization of materials

The ceramic ferroxanes were characterized by X-ray diffraction (XRD) using a PW1730-10 Diffractometer (Phillips). The specific surface area was measured by Brunauere–Emmette–Teller (BET) N_2 method and the pore size was calculated by the Barrett, Joyner and Halenda (BJH) N_2 adsorption/desorption isotherm method at 77 K using a Coulter SA 3100 (Beckman Coulter, USA) analyzer. The size of the bacteriophage P22 was determined by transmission electron microscopy (TEM) on a Philips EM301, and by dynamic light scattering using a Zetasizer Nano ZS (Malvern, UK); the same equipment was used for laser Doppler velocimetry measurements to characterize the electrophoretic mobility (EPM) of the bacteriophage and iron oxide particles. Measured EPMs were converted to zeta-potential using the Smoluchowski equation [33].

$$U = \varepsilon\xi/\mu \quad (8)$$

where U is the electrophoretic mobility, ε is the dielectric constant of the solution, μ is its viscosity, and ζ is the zeta potential. Disposable folded capillary cells were employed.

Attachment experiments

Attachment kinetics

The kinetic investigation of virus deposition onto hematite was performed in 45 mL sterile centrifuge tubes. A mass of 0.100 g of iron oxide was added to the tubes. Stirred and unstirred control experiments, as well as without iron oxide, were also conducted. An orbital shaker (M-23, Vicking) was set at a speed of 75 rpm, placing the tubes horizontally. The initial phage concentration in each tube was in the order of 10^7 pfu/mL. Samples were taken at different time intervals for 48 h.

Adsorption isotherms

Attachment experiments were carried out in sterile centrifuge tubes of 45 mL, where a determined mass of iron oxide ceramic was added, ranging from 0.010 to 0.150 g. Each tube was then filled with NaCl (Anedra) solution and sterilized. After this, the samples were inoculated with 0.100 mL of virus stock suspension of 10^{10} pfu/mL, reaching a concentration of approximately 10^7 pfu/mL. In parallel, two control experiments were carried out without the addition of iron oxide, one stirred and one unstirred, in order to evaluate the natural inactivation of the virus and quantify the effect of shear in the reduction of the number of pfu. The tubes were shaken in horizontal position in an orbital shaker (M-23, Vicking) at 75 rpm at room temperature for 7 h. Samples were taken from each batch at the beginning and at the end of each experiment.

Filtration experiments

The operational set-up used for the attachment during filtration experiments is shown schematically in Fig. 1. It consisted of an alumina-supported iron oxide ceramic tube with a dead end. This type of membrane was fabricated by depositing the iron oxide particles onto the alumina supports and was previously applied to the adsorptive filtration of inorganic contaminants [9]. Briefly, a suspension of the nanoparticles was filtered inside-out through the support tubes with one end closed so that all the water was forced through the ceramic, while the iron oxide particles were retained (Fig. 1a). The filter was then dried and sintered at 450 °C, before treatment of virus suspensions. Between 250 and 300 mL of viral solution was passed through a supported filter as shown in Fig. 1b. The feed solution entered inside the tube, forcing it to flow tangentially through the iron oxide coated walls. The permeate was sampled and tested for virus concentration. The original apparatus consisted of a 350 mL glass burette with Teflon stopcock and a short silicon hose attached to its bottom end. The supported filter could be attached at the distal end of the silicon hose. The top end of the burette was covered with a 22 μm Whatman filter and wrapped with aluminum foil to keep it in place. The tube filter alternatively placed into different Erlenmeyer flasks to obtain the subsequent aliquots, and was covered at all times by aluminum foil to minimize exposure to airborne contaminants. For the recirculation experiments, the same apparatus was used with some modifications. The hose was in this case long enough to pass through the peristaltic pump and then return to the top end of the burette. The supported filter could be attached at the distal end of the silicon hose, or alternatively the distal end could be left without any tube attached, according to the type of experiment performed. The top end of the burette was wrapped in sterile aluminum foil to prevent airborne particles from contaminating the system. The flow was set at a rate of about 0.38 mL/min, accounting for about 4 recirculation cycles per hour during a 48 h period. Samples were taken at different times during the experiment to assess the temporal evolution of virus concentration in the solution. The potential inactivation effect of the alumina tube itself was investigated in an experiment using an alumina tube with the same dimensions and characteristics of the sintered tube, but with no iron loaded onto it. In order to rule out viral inactivation due to stresses generated during the recirculation process, another run was performed with no tube in place.

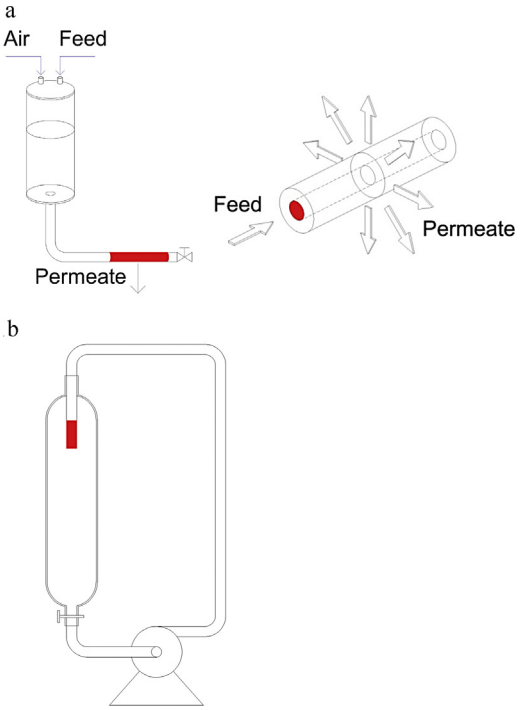

Fig. 1. Experimental set up for (a) supported filter fabrication; (b) dynamic filtration experiments.

Analytical methods

Two methodologies were applied to the determination of the concentration of P22 phage in the samples: agar layer method [36], and quantitative polymerase chain reaction (qPCR). For the double layer method, 3 mL of melted soft agar L was cooled to 45 °C and inoculated with 50 μL of concentrated suspension of *Salmonella* typhimurium DA1468 strain. Secondly, 0.1 mL of the phage suspension was added and the entire mixture was poured over the surface of a Petri dish with agar L. When needed, dilutions of the bacteriophage aliquots were made based on estimations and previous results. Once the top agar layer had solidified, the plate was incubated for 24 h at 37 °C. Finally, the plaques were counted, taking as valid the measurements those displaying between 30–300 plaques per dish.

The qPCR method was performed extracting DNA from 200 μL of P22 suspensions using the Pure Link Viral RNA/DNA Mini Kit (Invitrogen, Carlsbad, CA). The DNA was detected using a GeneAmp 5700 Sequence Detection System (Applied Biosystems, Foster City, California, US). The genomic sequence of the primers and probe used is described in the Table 2[37]. PCR mixtures (20 μL in total) contained 5 μL of DNA sample, 12.5 μL of 2X PCR master mix (TaqMan Universal Master Mix II, no UNG; Applied Biosystems, Indianapolis, IN), 500 nM each of forward and reverse primers, and 150 nM of the TaqMan probe. Amplification was initiated using the hot start method at 95 °C for 10 min; 40 cycles of 95 °C for 15 s, and 60 °C for 1 min. The detection limit was calculated to be 10 bacteriophages per sample.

DLVO modeling

The bacteriophage P22 was considered to have a perfect spherical geometry; the interaction between two spheres was modeled with Eqs. (1), (5) and (7). The needed parameters were calculated with Eqs. (2) and (3).

The ceramic membrane was regarded as an infinite plate compared to the virus P22 and the interaction between the plate and one sphere was calculated using Eqs. (4), (6) and (7), with the aid of Eqs. (2) and (3) to calculate the required parameters.

The Hamaker constants employed were: $A_{11} = 8.54 \times 10^{-20}$ J [33]; $A_{22} = 1.59 \times 10^{-19}$ J; $A_{33} = 3.70 \times 10^{-20}$ J. Then, upon calculations: $A_{132} = 2.06 \times 10^{-20}$ J and $A_{131} = 9.98 \times 10^{-21}$ J were derived [38–40].

Table 2
Primer and probe sequences for detection of P22.

Target	Name	Sequence	Reference
P22	P22-2F	CTT AAC AAG CTC TGA CTG CTC ATC A	Masago et al., 2008
	P22-2R	CCA TCG CCT GTG ACT GGA T	
	P22-2P	FAM-TCG CAA CGA TGC AGA ACG ACT CG-TAMRA	

Results and discussion

Materials characterization

The ferroxane particles were sintered at 450 °C, in order to convert to the nanoporous ceramic, and characterized. XRD showed that the iron oxide was completely converted to hematite, α-Fe_2O_3. BET specific surface area from nitrogen adsorption isotherms was determined to be $29.3 \pm 1.5\ m^2/g$. Pore size distribution calculated from the adsorption branch of isotherm yielded a mean pore size of 62 nm and a standard deviation of the distribution of 40 nm.

P22 and ferroxane-derived iron oxide surface charge was measured as a function of pH (Fig. 2). The isoelectric point, represented by the pH at which the phages have no net surface charge, was estimated from the data points where the electrophoretic mobility changes from positive to negative. With an IEP of 3.4, the virus is expected to be negatively charged under the conditions of environmentally relevant pHs, reaching a value of −27.9 mV at pH 7, and remaining relatively stable for alkaline solutions. The ferroxane derived ceramic showed a point of zero charge (pzc) of 6, in agreement with previously published values for hematite [41]. Consequently, the virus will be subjected to attractive interaction forces at pHs below 6, while attachment is expected to be hampered by electrostatic repulsion at higher pHs.

Virus size was measured by DLS and TEM. DLS analysis gave a hydrodynamic diameter of 71 ± 0.8 nm, while analysis of TEM images suggested a size of 58 ± 9 nm.

Virus attachment

Virus concentration was determined by two methodologies: pfu and qPCR. The former was applied to all samples, due to availability to the technique in our laboratory and relevancy. Pfu determinations only accounts for active or infective organisms, since it relies on the quantification of the damage caused by the phage suspension to the host bacteria. However, the technique suffers from the drawback of possible underestimating the real virus concentration, if the microorganisms happen to be aggregated in the sample, and therefore the assumption that each plaque correspond to a single viral particle would not hold [42]. The qPCR measurements are sensitive to all P22 genetic material, and report on both infective and inactivated viruses, which may lead to an overestimation of the infective capability of the suspension but it is not affected by the physico-chemical properties of the media or the aggregation state of the viral particles [43]. In order to analyze the quality of the pfu determinations conducted in this work, a P22 suspension was analyzed under changing conditions of pH and ionic strength, given in all cases by the NaCl, and the results from both methods compared. Fig. 3 shows measurements of P22 concentration by qPCR and pfu for pH values between 4 and 7. For the full range of pHs investigated, P22 have a net negative surface charge as evidenced by the zeta potential measurement (Fig. 2). This surface potential would result effective in preventing aggregation at all investigated pHs but pH 4, where the zeta potential absolute value is only slightly over 5 mV. Virus determinations by pfu technique gave steady results over a range of pHs of 5–7, and less than an order of magnitude lower for pH 4. This difference may be due in part to some aggregation of the viral particles when repulsion forces are weaker. The comparison with qPCR results showed excellent agreement for pH 7. At neutral conditions, pH

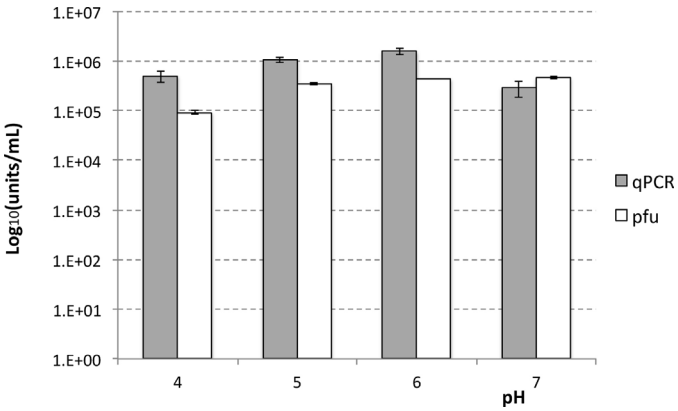

Fig. 3. Determination of virus concentration under different pHs; gray: results by qPCR; white: results by pfu.

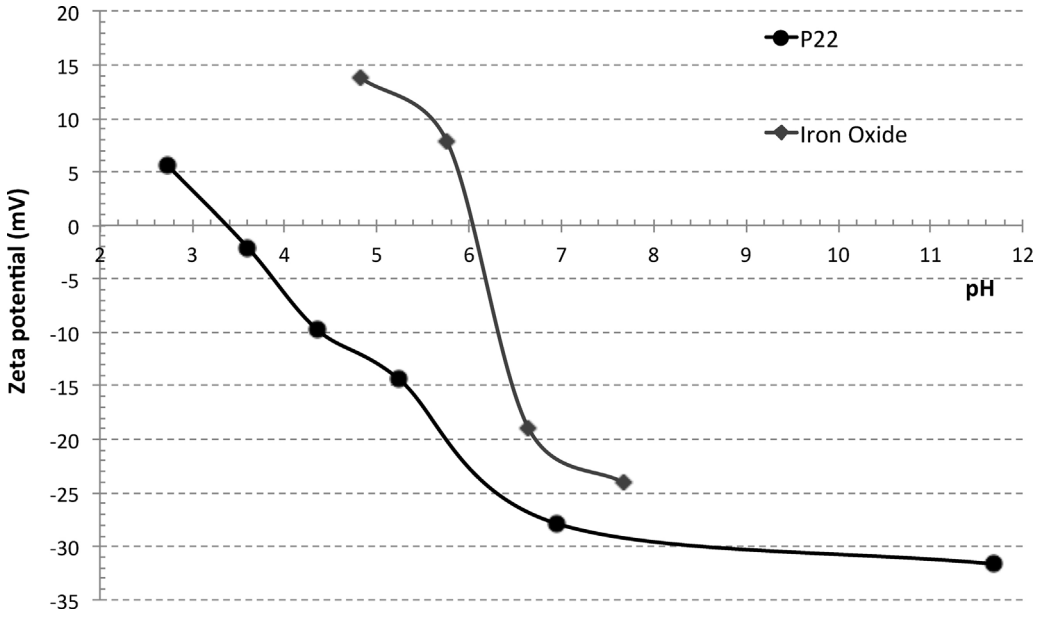

Fig. 2. Zeta potential as a function of pH for: P22 bacteriophage, ionic strength 15 mM of NaCl, $T = 20$ °C; and nanostructured iron oxide, ionic strength 15 mM of NaCl, $T = 20$ °C.

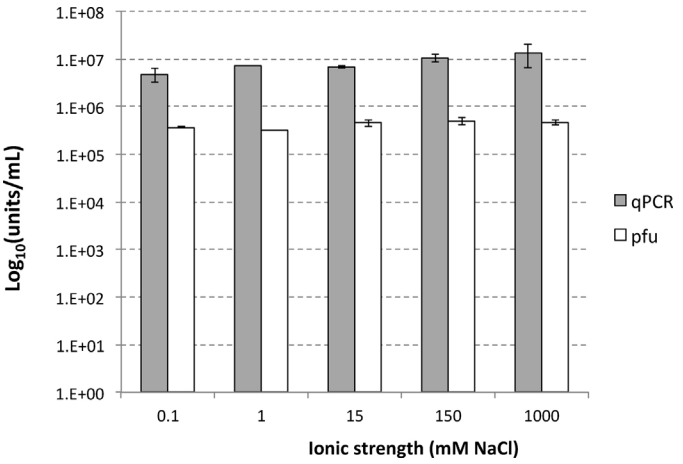

Fig. 4. Determination of virus concentration under different ionic strength levels; gray: results by qPCR; white: results by pfu.

related inactivation is expected to be negligible; also, the highest absolute value of zeta potential is observed at pH 7, and therefore aggregation should be minimal, if any. Based on this considerations and the experimental error associated with the data, we concluded that the measurements for both techniques were equivalent. At lower pHs, a reduction in the concentration determined by pfu compared to the qPCR obtained values is observed, especially for pH 4, probably as a combination of two effects: partial aggregation as surface potential become less negative, and the acidic conditions affecting the organism viability [44,45]. The effect of ionic strength on the quantification method was also investigated, and plotted in Fig. 4. Results showed good agreement between analytical methods, and no appreciable difference can be observed between 0.1 mM and 1 M NaCl suspensions. Increasing ionic strength is expected to induce aggregation as electric double layer compression results in shorter-range repulsive forces and overall dominance of van der Waals attractive interaction, but no significant virus aggregation can be inferred form the experimental results. Furthermore, qPCR determinations were in all cases uniformly higher than pfu, hinting to the presence of some inactive viruses in all of the measured samples.

Overall, it can be concluded that both techniques can be applied to accurate quantification of virus concentration in the present study with minor underestimations by pfu method at lower pH levels.

Attachment kinetics

Attachment kinetics experiments were conducted in order to investigate the time and evolution of the attachment process as well as to determine the appropriate equilibration time to be used in the isotherm determination.

Samples were analyzed by pfu technique. Given that some degree of inactivation may occur when virus are subjected to stirring or room temperature, two control experiments were added to determine the relative contribution to the loss of viral activity due to these factors.

Fig. 5 presents the results from the kinetics experiments. Samples containing virus and iron oxide were obtained (E); SC data points correspond to the stirred virus suspension without the addition of adsorbent and (C) relates to the same sample composition without stirring. In the first 7 h an average log removal of 1.4 was observed for the samples containing the adsorbent, while no detectable reduction in virus concentration was observed for the control experiments. The decrease in log reduction values (LRV) of virus concentration continued, but inactivation in the control samples started at 24 h, and therefore the LRV could not be attributed entirely to attachment to the iron oxide particles.

Fig. 6 depicts the net amount of virus expected to be adsorbed on the iron oxide, calculated from the measured virus concentration and subtracting the effect of room temperature and shear due to stirring on inactivation as determined by the control experiments. A rapid decrease in virus concentration is observed in the first 7 h, followed by a marginal increase in removal up to the 48 h time frame of the experiment. This may hint to a two phase process, when a rapid removal is observed corresponding to the readily available easier to reach surface sites for the iron oxide, and a second, much slower stage in which the adsorbate diffuses into the internal structure of the iron oxide particles finding new sites.

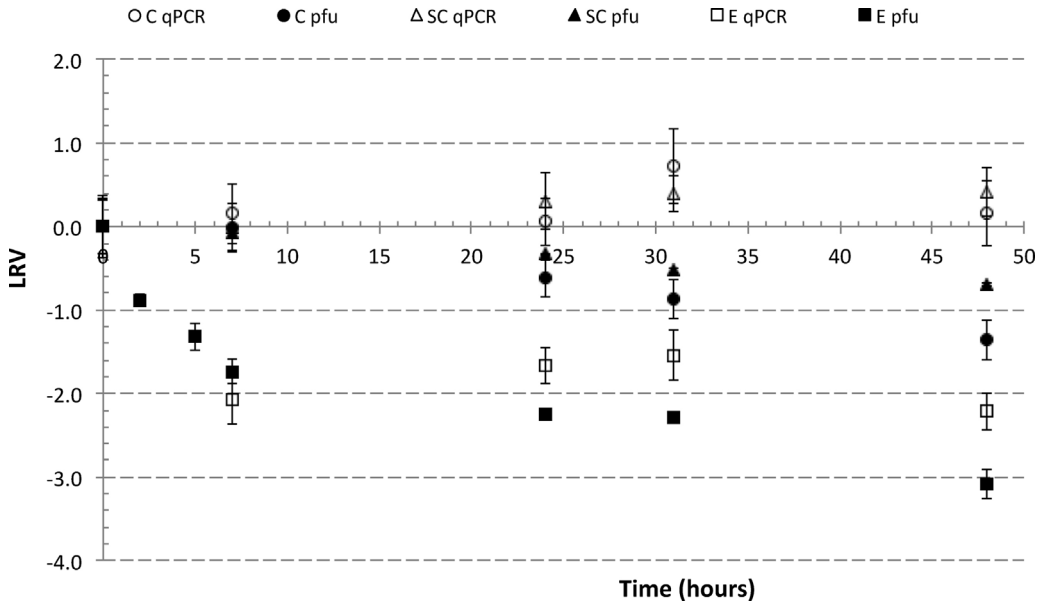

Fig. 5. Logarithmic reduction value (LRV) of bacteriophage P22 concentration (Co = 10^7 pfu/mL) as a function of time in the presence of iron oxide (2 μg/mL), analyzed by qPCR and pfu methods; E: virus and adsorbent; SC, C: no adsorbent control samples, stirred and unstirred respectively.

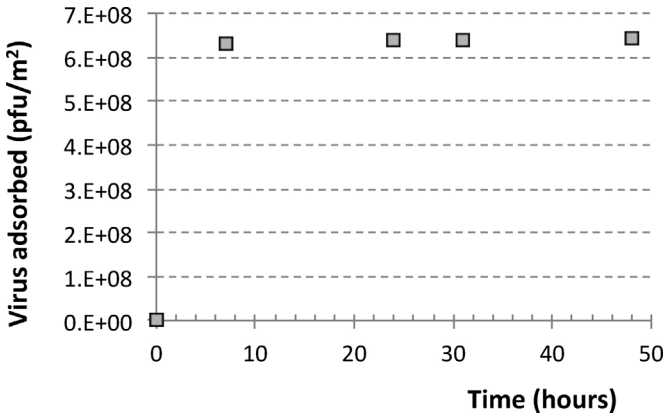

Fig. 6. Adsorption kinetics of bacteriophage P22 (Co = 10^7 pfu/mL) on iron oxide particles (2 μg/mL); inactivation due to environmental conditions was subtracted to obtain net adsorption values.

A similar behavior has been observed for ionic species adsorbing to nanoporous materials [46,47] and in particular, for arsenite adsorption onto this same iron oxide particles [9]. In fact, BJH pore volume distribution from nitrogen adsorption isotherms showed that about one third of the total pore volume of the iron oxide particles is given by pores larger than 65 nm, and 27% of those are within the 54–120 nm range. Thus, this internal surface area is available at least in part to the virus that given its size of approximately 70 nm, as measured in this work and in consistency this literature [29–31], is able to diffuse into the nanostructure and adsorb into the pore walls. However, the process is expected to be much slower than for the ionic species due to the limited diffusion and possible pore clogging by previous adsorbed particles, and therefore a very slow reduction in concentration is observed, rending this stage not suitable for engineering applications. We have therefore assumed a pseudo-equilibrium state is reached after 7 h contact time and adopted this time for all subsequent experiments.

The results are similar or better than previously reported adsorbent materials for virus removal. For example, with an initial virus concentration of 10^7 pfu, Gutierrez et al. reported adsorption of MS2 on hematite nanoparticles to be less than 2 log removal units after 3 h contact time from simulated groundwater and similar adsorbent dose to the one used in this work [20]; in another work, iron oxide magnetic nanoparticles achieved 0.36 log removal units in 60 min at 2 g/L concentration [48].

Adsorption isotherm

Attachment experiments were carried out adding a determined mass of iron oxide ceramic ranging from 0.010 to 0.150 g to a sterile NaCl solution following by inoculation with 0.100 mL of virus stock suspension of 10^{10} pfu/mL to reach a concentration of approximately 10^7 pfu/mL. Experiments without iron oxide addition and unstirred were also implemented as controls to quantify inactivation by mechanical shear and exposition at room temperature. Samples were taken at the beginning and after 7 h of contact time.

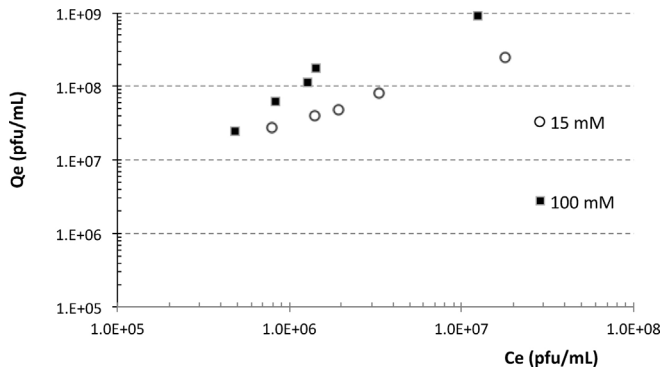

Fig. 7. Adsorption isotherm for P22 bacteriophage on nanostructured iron oxide; T = 25 °C, electrolyte concentration 15 and 100 mM NaCl.

The obtained attachment isotherm at 25 °C is shown in Fig. 7, at two different levels of ionic strength, 15 and 100 mM NaCl. Virus may be present in different waters: surface water, groundwater, seawater, wastewaters, and they all present different levels of ionic strength. Moreover, being the attachment of virus to iron oxide electrostatic in nature, ionic strength is expected to play a fundamental role, making its investigation highly relevant. The data points showed the net loss of virus activity due to attachment onto iron oxide, as the inactivation levels observed in the controls have been subtracted to the reported values. The results showed increases of the adsorbed concentration with increasing liquid equilibrium concentration for the range of conditions tested. A plateau was not reached, although the slope showed a slight decrease for the highest concentration point. The isotherms were fit to the linearized from of three model isotherms: Langmuir, Freundlich, and Temkin and the corresponding coefficients of determination (R^2) calculated (Table 3). The three proposed equations depict relatively well the experimental data, the Freundlich isotherm showing the highest goodness of fit. Additionally, the absence of a plateau in the curves that could be related to the surface sites saturation suggests the inappropriateness of both Langmuir and Temkin equations, even though the data fit relatively well the first linear portion of the corresponding isotherms. The Freundlich equation is often used to describe cation adsorption data on iron oxides [41]; however this equation is purely empirical and provides no information on the adsorption mechanism. The data analysis is useful for comparison purposes: the ferroxane-derived ceramics showed higher adsorption when ionic strength, given by NaCl, is increased from 15 to 100 mM; the increased affinity in the 100 mM case is also reflected in a higher n value.

This dependence hints to an electrostatic interaction mechanisms for virus attachment, regulated by van der Waals and electrostatic repulsion forces, which can be altered by the concentration of salts in the water matrix.

Filtration experiments

A virus suspension with similar concentration as tested for the batch experiments, was filtered through ferroxane-coated alumina filters. This breakthrough experiment as originally conceived did not yield a measurable reduction in the viral load of the solution. This may be due to a low attachment efficiency of the P22 under the conditions tested, that cause a significant number of particles to pass through the ceramic filter without being retained; other reason for the poor performance may be related to the relatively open pore structure of the ceramic support, that offer short cuts for the particles to flow through the filter and drastically diminished the occurrence of collisions with potential attachment sites. Consequently, a rearrangement of the supported filter setup was carried out. A peristaltic pump was added to the circuit in order to recirculate the filtrate back to the feed burette. The speed was set in

Table 3
Model fits for virus adsorption isotherms.

	Ionic strength	Langmuir	Temkin	Freundlich		
		R^2	R^2	R^2	K_f	n
P22	15 mM of NaCl	0.9776	0.9373	0.9974	1.44E2	0.724
	100 mM of NaCl	0.9355	0.9549	0.9415	39.0	1.02

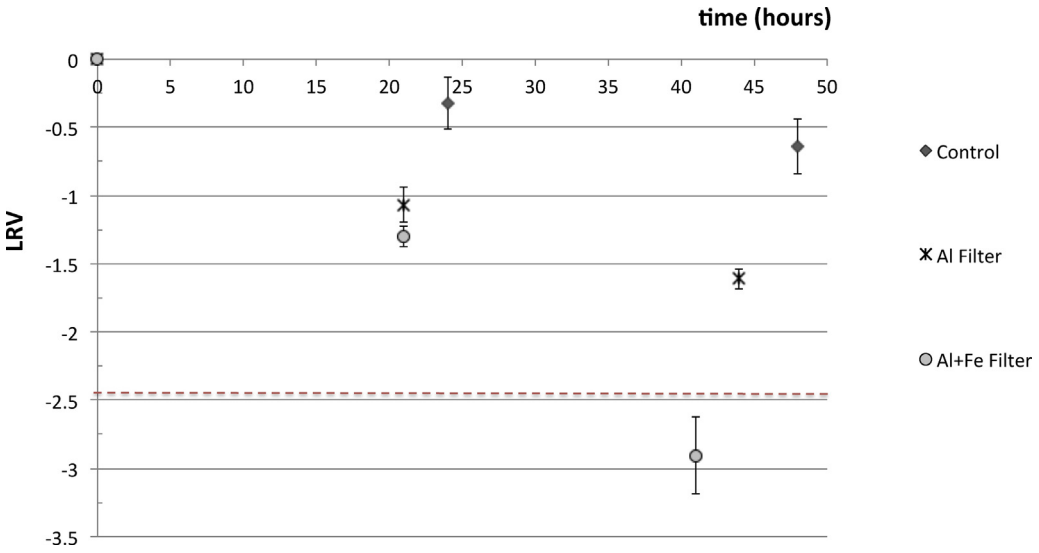

Fig. 8. Logarithmic reduction values of P22 by recirculation of a feed solution through a ferroxane-coated alumina filter.

such a way that approximately 4 recirculation cycles were performed every hour, increasing the residence time.

Results showed (Fig. 8) that viral attachment/inactivation is strongly dependent on the time elapsed since the beginning of the experiment. In the case of the ferroxane-loaded tube, the concentration of viable viral particles dropped close to the detection limit at the end of the 48 h test period. The alumina tube seems to be effective as well in reducing the viable viral load of the solution, although less than in the case of the iron-oxide loaded tube. In comparison, the experiments performed without filter showed a much lesser degree of inactivation, within a range of values that can wholly or partly be due to the expected measurement error, indicating that shear due to pumping is not a significant contributor to virus inactivation.

DLVO theory analysis of virus attachment

Since electrostatic interactions are expected to dominate the virus attachment to metal oxide surfaces, DLVO theory was applied to the analysis of the attachment data as well as the virus stability and aggregation conditions.

Bacteriophage P22 particles were modeled as spheres with a diameter of 71 nm, while the adsorbent was modeled as a plate due to the larger dimensions in comparison with the P22.

Fig. 9 shows the interaction potential energy for two bacteriophage P22 particles in a pH range of 3–7, and a background ionic strength of 15 mM. At low values of pH (i.e., 3 and 4), van der Waals interaction energy completely overweighs electrical double layer interaction energy, and a net attraction potential and thus

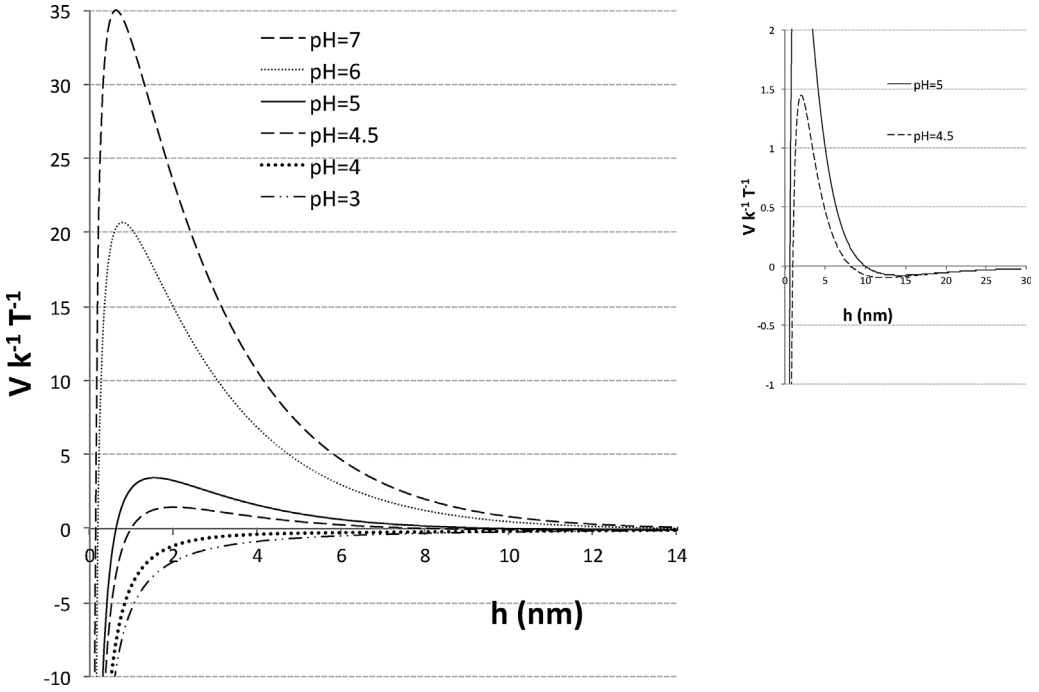

Fig. 9. DLVO predicted interaction potentials for two P22 bacteriophages, modeled as 71 nm spheres, in a 15 mM (NaCl) ionic strength media, for pH range between 3 and 7. Inset shows secondary minimum present at pH 4.5 and 5.

aggregation between the particles is expected. At pHs close to neutral, an energy barrier develops such that aggregation may be effectively prevented. At intermediate pHs, illustrated here by the pH 4.5 and 5 calculations, a low barrier in the total energy is present. A fraction of the particles may overcome this barrier due to energy associated with Brownian motion and aggregate in the primary minimum in a similar fashion as in the low pH conditions; additionally, particles may aggregate in a secondary minimum that develops at these intermediate pH values but these weaker structures are highly likely to release individual particles [33]. The comparison of concentration measurements by pfu and qPCR techniques (Fig. 3) showed equivalent determinations at pH 7, and relatively lower values given by pfu for pH 4, 5 and 6, the former showing the larger difference. In light of the DLVO calculations, we can explain the difference at the two middle points by limited aggregation due to a moderate to low energy barrier; however, the predicted instability at pH 4 does not agree with the measured results, that did not revealed a significant difference between both techniques and therefore, not extensive aggregation can be concluded. The results suggested an underestimation of the repulsive forces by the DLVO theory as applied in this study.

The interaction potential between the iron oxide ceramic and the P22 particles were analyzed based on DLVO calculations for pHs between 4 and 7 (Fig. 10). The results showed a strong dependence of attachment on pH. For pH values 4 to 6, a deep primary minimum in the interaction energy is predicted, and strong attachment is expected. As pH gets closer to the point of zero charge of the adsorbent, repulsive forces arise. A moderate energy barrier is predicted at pH 6.5, while unfavorable conditions for deposition develop at pH 7. If virus repulsive forces are underestimated as suggested by the discussion above, the applicability of the method could be further limited to pHs below 6.5.

Divergence between DVLO predicted stability and experimental observations are commonly attributed to non-DLVO interactions, e.g., Born repulsion, hydration forces, hydrophobic and/or steric forces, polymer bridging. Of these, only hydration forces may be postulated. Although their effect is anticipated to be comparable to double layer repulsion at higher ionic strengths than those considered in this study [49], they explained MS2 and φX174 attachment to clay particles [50]. Another limitation to the application of the DLVO theory arises from the fact that virus particles can be defined as soft particles, e.g., particles covered with ion-penetrable surface layer of polyelectrolytes, as opposed to hard particles where the surface is clearly defined and no electrolyte ions can penetrate it [51].

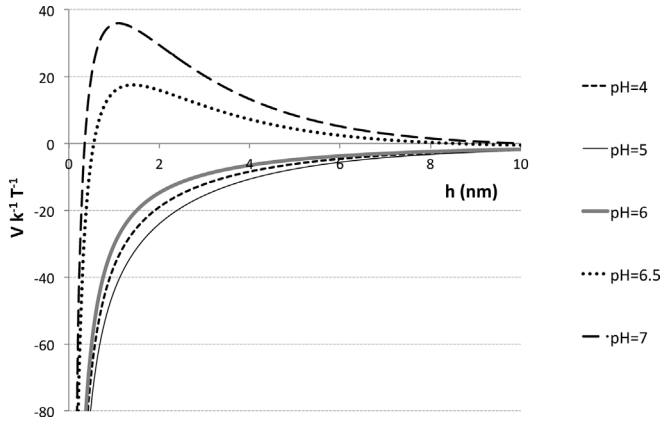

Fig. 10. DLVO predicted interaction potentials for P22 bacteriophages and the iron oxide membrane; modeled as sphere-plate system; 15 mM (NaCl) ionic strength, pH range between 4 and 7.

Conclusion

Iron oxide ceramic membranes were successfully applied for the removal of virus from water. Iron oxide coated alumina filters showed improved removal capacity compared to the stand-alone material tested in batch mode, as inner pore sites that otherwise would be considered inaccessible due to long diffusion times become operational. Additional improvement can be achieved by the design of a support material with more uniform porosity, avoiding the possibility of wide channels inside the pore structure that result in inefficiency in the attachment process. The recirculation required in the filtration experiments constitutes a barrier for cost-effective application of the technology in a water treatment plant scenario. Therefore, an increase in the efficiency of the removal at each cycle is needed. This can be achieved by an improved the support porosity, that enhances the contact between the solution and the iron oxide-coated walls. The optimization of the support material will be the subject of future work. The mechanism of removal was observed to be electrostatic in nature. DLVO analysis of the attachment predicted it to be effective up to a pH of 6.5. The filters are especially applicable as a mobile drinking water treatment device, due to their low cost, ease of use and extra capabilities of the membrane, such as the removal of organic contaminants or heavy metals.

References

[1] M.A. Borchardt, S.K. Spencer, B.A. Kieke Jr., E. Lambertini, F.J. Loge, Viruses in nondisinfected drinking water from municipal Wells and community incidence of acute gastrointestinal illness, Environ. Health Perspect. 120 (2012) 1272–1279, doi:http://dx.doi.org/10.1289/ehp.1104499. 22659405.

[2] A.M. ElHadidy, S. Peldszus, M.I. Van Dyke, An evaluation of virus removal mechanisms by ultrafiltration membranes using MS2 and φX174 bacteriophage, Sep. Purif. Technol. 120 (2013) 215–223.

[3] S.R. Farrah, C.P. Gerba, C. Wallis, J.L. Melnick, Concentration of viruses from large volumes of tap water using pleated membrane filters, Appl. Environ. Microbiol. 31 (1976) 221–226. 187115.

[4] M. Mulder, Basic Principles of Membrane Technology, Kluwer Academic, Dordrecht, The Netherlands, 1996.

[5] L.T. Chang, S.R. Farrah, G. Bitton, Positively charged filters for virus recovery from wastewater treatment plant effluents, Appl. Environ. Microbiol. 42 (1981) 921–924. 6274257.

[6] C.P. Gerba, J.C. Lance, Poliovirus removal from primary and secondary sewage effluent by soil filtration, Appl. Environ. Microbiol. 36 (1978) 247–251. 211936.

[7] J. Rose, M.M. Fidalgo de Cortalezzi, S. Moustier, C. Magnetto, C. Jones, A. Barron, M. Wiesner, J.-Y. Bottero, Synthesis and characterization of carboxylate-FeOOH particles (ferroxanes) and ferroxane-derived ceramics, Chem. Mater. 14 (2002) 621–628.

[8] M.M.F.d. Cortalezzi, J. Rose, G. Wells, J.-Y. Bottero, M. Wiesner, Ceramic membranes derived from ferroxane nanoparticles: a new route for the fabrication of iron oxide ultrafiltration membranes, J. Membr. Sci. 227 (2003) 207–217.

[9] P. Sabbatini, F. Yrazu, F. Rossi, G. Thern, A. Marajofsky, M.M. Fidalgo de Cortalezzi, Fabrication and characterization of iron oxide ceramic membranes for arsenic removal, Water Res. 44 (2010) 5702–5712, doi:http://dx.doi.org/10.1016/j.watres.2010.05.059. 20599241.

[10] P. Christian, A. Richards, R.A. Williams, Differential adsorption of occluded and nonoccluded insect-pathogenic viruses to soil-forming minerals, Appl. Environ. Microbiol. 72 (2006) 4647–4652.

[11] S. Wang, H.M. Ang, M.O. Tadé, Novel applications of red mud as coagulant, adsorbent and catalyst for environmentally benign processes, Chemosphere 72 (2008) 1621–1635, doi:http://dx.doi.org/10.1016/j.chemosphere.2008.05.013. 18558418.

[12] R. Flynn, R. Taylor, R. Kulabako, M. Miret-Gaspa, Haematite in lateritic soils aids groundwater disinfection, Water Air Soil Pollut. 223 (2012) 2405–2416.

[13] J. Meschke, M. Sobsey, Comparative adsorption of Norwalk virus, poliovirus 1 and F+RNA coliphage MS2 to soils suspended in treated wastewater, Water Sci. Technol. 38 (1998) 187–189.

[14] C.P. Gerba, E.M. Smith, J.L. Melnick, Development of a quantitative method for detecting enteroviruses in estuarine sediments, Appl. Environ. Microbiol. 34 (1977) 158–163. 20839.

[15] M.D.B. Fernández, C. Torres, H.R. Poma, G. Riviello-López, L.C. Martínez, D.M. Cisterna, V.B. Rajal, S.V. Nates, V.A. Mbayed, Environmental surveillance of norovirus in Argentina revealed distinct viral diversity patterns, seasonality and spatio-temporal diffusion processes, Sci. Total Environ. 437 (2012) 262–269, doi:http://dx.doi.org/10.1016/j.scitotenv.2012.08.033. 22944218.

[16] I. Bradley, A. Straub, P. Maraccini, S. Markazi, T.H. Nguyen, Iron oxide amended biosand filters for virus removal, Water Res. 45 (2011) 4501–4510, doi:http://dx.doi.org/10.1016/j.watres.2011.05.045. 21708394.
[17] J.A. Park, J.H. Kim, J.K. Kang, J.W. Son, I.G. Yi, S.B. Kim, Flow-through experiments for bacteriophage MS2 removal by iron oxide-impregnated fiberglass, Desalin. Water Treat. (2014).
[18] B.M. Pecson, L. Decrey, T. Kohn, Photoinactivation of virus on iron-oxide coated sand: enhancing inactivation in sunlit waters, Water Res. 46 (2012) 1763–1770, doi:http://dx.doi.org/10.1016/j.watres.2011.12.059. 22264797.
[19] J.N. Ryan, R.W. Harvey, D. Metge, M. Elimelech, T. Navigato, A.P. Pieper, Field and laboratory investigations of inactivation of viruses (PRD1 and MS2) attached to iron oxide-coated quartz sand, Environ. Sci. Technol. 36 (2002) 2403–2413.
[20] L. Gutierrez, X. Li, J. Wang, G. Nangmenyi, J. Economy, T.B. Kuhlenschmidt, M.S. Kuhlenschmidt, T.H. Nguyen, Adsorption of rotavirus and bacteriophage MS2 using glass fiber coated with hematite nanoparticles, Water Res. 43 (2009) 5198–5208, doi:http://dx.doi.org/10.1016/j.watres.2009.08.031. 19766286.
[21] G. Nangmenyi, X. Li, S. Mehrabi, E. Mintz, J. Economy, Silver-modified iron oxide nanoparticle impregnated fiber glass for disinfection of bacteria and viruses in water, Mater. Lett. 65 (2011) 1191–1193.
[22] J. Brown, M.D. Sobsey, Ceramic media amended with metal oxide for the capture of viruses in drinking water, Environ. Technol. 30 (2009) 379–391, doi:http://dx.doi.org/10.1080/09593330902753461. 19492549.
[23] B. Michen, J. Fritsch, C. Aneziris, T. Graule, Improved virus removal in ceramic depth filters modified with MgO, Environ. Sci. Technol. 47 (2013) 1526–1533, doi:http://dx.doi.org/10.1021/es303685a. 23286835.
[24] S.R. Farrah, D.R. Preston, Adsorption of viruses by diatomaceous earth coated with metallic oxides and metallic peroxides, Water Sci. Technol. 24 (1991) 235–240.
[25] W. Grabow, Bacteriophages: update on application as models for viruses in water, Water SA 27 (2001) 251–268.
[26] J.J. Dennehy, Bacteriophages as model organisms for virus emergence research, Trends Microbiol. 17 (2009) 450–457, doi:http://dx.doi.org/10.1016/j.tim.2009.07.006. 19765997.
[27] C. Shen, M.S. Phanikumar, T.T. Fong, I. Aslam, S.P. McElmurry, S.L. Molloy, J.B. Rose, Evaluating bacteriophage P22 as a tracer in a complex surface water system: the Grand river, Michigan, Environ. Sci. Technol. 42 (2008) 2426–2431.
[28] C.V. Chrysikopoulos, A.F. Aravantinou, Virus attachment onto quartz sand: role of grain size and temperature, J. Environ. Chem. Eng. 2 (2014) 796–801.
[29] S.R. Casjens, Molecular organization of the bacteriophage P22 coat protein shell, J. Mol. Biol. 131 (1979) 1–19. 385887.
[30] J. Chang, P. Weigele, J. King, W. Chiu, W. Jiang, Cryo-EM asymmetric reconstruction of bacteriophage P22 reveals organization of its DNA packaging and infecting machinery, Structure 14 (2006) 1073–1082, doi:http://dx.doi.org/10.1016/j.str.2006.05.007. 16730179.
[31] W. Earnshaw, S.R. Casjens, S.C. Harrison, Assembly of the head of bacteriophage P22: X-ray diffraction from heads, proheads and related structures, J. Mol. Biol. 104 (1976) 387–410. 781287.
[32] J. Gregory, Interaction of unequal double layers at constant charge, J. Colloid Interface Sci. 51 (1975).
[33] M. Elimelech, J. Gregory, X. Jia, R.A. Williams, Particle Deposition and Aggregation – Measurement, Modelling and Simulation, Butterworth-Heinemann, Woburn, Massachussets, USA, 1995.
[34] H.C. Hamaker, The London – van der Waals attraction between spherical particles, Physiology 4 (1937) 1058–1072.
[35] I.T. Kudva, S. Jelacic, P.I. Tarr, P. Youderian, C.J. Hovde, Biocontrol of *Escherichia coli* O157 with O157-specific bacteriophages, Appl. Environ. Microbiol. 65 (1999) 3767–3773. 10473373.
[36] M. Adams, Bacteriophages, Interscience Publishers, Inc., London, 1959.
[37] Y. Masago, T. Shibata, J.B. Rose, Bacteriophage P22 and *Staphylococcus aureus* attenuation on nonporous fomites as determined by plate assay and quantitative PCR, Appl. Environ. Microbiol. 74 (2008) 5838–5840, doi:http://dx.doi.org/10.1128/AEM.00352-08. 18621868.
[38] F.L. Leite, C.C. Bueno, A.L. Da Róz, E.C. Ziemath, O.N. Oliveira Jr, Theoretical models for surface forces and adhesion and their measurement using atomic force microscopy, Int. J. Mol. Sci. 13 (2012) 12773–12856, doi:http://dx.doi.org/10.3390/ijms131012773. 23202925.
[39] B. Gilbert, G. Lu, C.S. Kim, Stable cluster formation in aqueous suspensions of iron oxyhydroxide nanoparticles, J. Colloid Interface Sci. 313 (2007) 152–159, doi:http://dx.doi.org/10.1016/j.jcis.2007.04.038. 17511999.
[40] T.K. Tokunaga, Physicochemical controls on adsorbed water film thickness in unsaturated geological media, Water Resour. Res. 47 (2011) W08514.
[41] R.M. Cornell, U. Schwertmann, The Iron Oxides: Structure, Properties, Reactions, Occurrences and Uses, second ed., Wiley-VCH Verlag GmbH & Co. KGaA, Weinheim, 2004.
[42] H. Adams, Bacteriophages, Interscience, New York, 1959.
[43] R. Girones, M.A. Ferrús, J.L. Alonso, J. Rodriguez-Manzano, B. Calgua, A.deA. Corrêa, A. Hundesa, A. Carratala, S. Bofill-Mas, Molecular detection of pathogens in water – the pros and cons of molecular techniques, Water Res. 44 (2010) 4325–4339, doi:http://dx.doi.org/10.1016/j.watres.2010.06.030. 20619868.
[44] C.M. Sabatino, S. Maier, Differential inactivation of three bacteriophages by acid and alkaline pH used in the membrane adsorption–elution method of virus recovery, Can. J. Microbiol. 26 (1980) 1403–1407. 7237265.
[45] M.K. Amin, M.J. Day, Influence of pH value on viability and transduction frequency of *Pseudomonas aeruginosa* phage F116, Lett. Appl. Microbiol. 6 (1988) 93–96.
[46] I.R. Willett, C.J. Chartres, T.T. Nguyen, Migration of phosphate into aggregated particles of ferrihydrite, J. Soil Sci. 31 (1988) 275–282.
[47] C.C. Fuller, J.A. Davis, G.A. Waychunas, Surface chemistry of ferrihydrite: part 2. Kinetics of arsenate adsorption and coprecipitation, Geochim. Cosmochim. Acta 57 (1993) 2271–2282.
[48] J.A. Park, S.B. Kim, C.G. Lee, S.H. Lee, J.W. Choi, Adsorption of bacteriophage MS2 to magnetic iron oxide nanoparticles in aqueous solutions, J. Environ. Sci. Health A Tox./Hazard. Subst. Environ. Eng. 49 (2014) 1116–1124, doi:http://dx.doi.org/10.1080/10934529.2014.897147. 24844892.
[49] T.W. Healy, A. Homola, R.O. James, R.J. Hunter, Coagulation of amphoteric latex colloids: reversibility and specific ion effects, Faraday Discuss. Chem. Soc. 65 (1978) 156–163.
[50] C.V. Chrysikopoulos, V.I. Syngouna, Attachment of bacteriophages MS2 and φX174 onto kaolinite and montmorillonite: extended-DLVO interactions, Colloids Surf. B Biointerfaces 92 (2012) 74–83, doi:http://dx.doi.org/10.1016/j.colsurfb.2011.11.028. 22153836.
[51] H. Ohshima, Electrokinetic phenomena of soft particles, Curr. Opin. Colloid Interface Sci. 18 (2013) 73–82.